ACS Catalysis

Letter

pubs.acs.org/acscatalysis

Intercalation of Cobalt into the Interlayer of Birnessite Improves Oxygen Evolution Catalysis

Akila C. Thenuwara,[†,§] Samantha L. Shumlas,[†,§] Nuwan H. Attanayake,[†,§] Yaroslav V. Aulin,[†,§] Ian G. McKendry,[†,§] Qiao Qiao,[‡,§] Yimei Zhu,[‡,§] Eric Borguet,[†,§] Michael J. Zdilla,[†,§] and Daniel R. Strongin*[,†,§]

[†]Department of Chemistry, Temple University, Beury Hall, 1901 North 13th Street, Philadelphia, Pennsylvania 19122, United States

[‡]Department of Condensed Matter Physics and Materials Science, Brookhaven National Laboratory, Upton, New York 11973, United States

[§]Center for the Computational Design of Functional Layered Materials (CCDM), Temple University, Philadelphia, Pennsylvania 19122, United States

Supporting Information

ABSTRACT: We show that the activity of cobalt for the oxygen evolution reaction (OER) can be enhanced by confining it in the interlayer region of birnessite (layered manganese oxide). The cobalt intercalation was verified by employing state-of-the-art characterization techniques such as X-ray diffraction, Raman spectroscopy, and electron microscopy. It is demonstrated that the Co^{2+}/birnessite electrocatalyst can reach 10 mA cm^{-2} at an overpotential of 360 mV with near-unity Faradaic efficiency. This overpotential is lower than that which can be achieved by using a pure cobalt hydroxide electrocatalyst for the OER. Furthermore, the Co^{2+}/birnessite catalyst shows no degradation after 1000 electrochemical cycles.

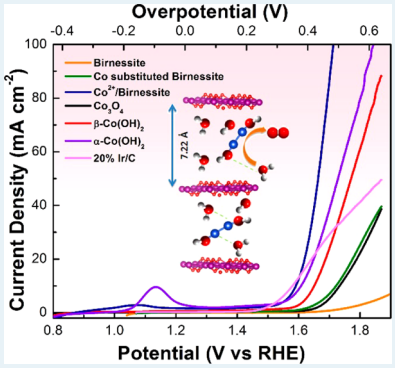

KEYWORDS: *oxygen evolution reaction, cobalt intercalation, birnessite, electrocatalyst, water splitting*

Implementation of sustainable and affordable clean energy technologies requires cheap and highly active (electro)-catalysts.[1] Among all renewable energy research, electrochemical and photoelectrochemical water splitting have been identified as promising fuel-producing reactions, although the reaction is hindered by sluggish kinetics.[2,3] Recent developments in renewable energy research have led to the discovery of highly active hydrogen evolution reaction (HER) catalysts with earth-abundant materials such as MoS_2, WS_2, CoP, Ni_3Se_2 with overpotentials (η) less than 100 mV.[4−7] Even the best precious-metal-based oxygen evolution reaction (OER) catalysts, IrO_2 and RuO_2, suffer from high overpotentials (>300 mV) and stability issues in alkaline media.[8,9] Recent research, however, in the context of lowering η for the OER, has shown that a ternary catalyst (FeCoW oxyhydroxide) exhibits a η of ∼200 mV for OER.[10]

Apart from heterogeneous water oxidation catalysts (WOC), molecular-based WOC have been extensively studied mainly due to the ease of designing well-defined catalytically active centers, which is convenient for elucidating reaction mechanisms.[11,12] Developments in molecular-based WOC research have been able to discover extremely active catalysts where the reported turnover frequency (>300 s^{-1}) is comparable with nature's WOC, photosystem II (PS II).[13] However, successful integration of these molecular-based catalysts into commercial water splitting devices is yet to be reported.

Numerous studies have investigated manganese-based materials for OER.[14−17] The motivation for these studies has in part been due to nature's use of manganese as an active component in the PS II cluster, which is known to perform water oxidation. As part of this prior research, birnessite, a material composed of two-dimensional layers of edge-sharing manganese octahedra (MnO_6), has been investigated. It has been shown that this layered material is a moderately active electrocatalyst for the OER.[16−21] Compared to other manganese oxide phases, however, birnessite is one of the least active materials, exhibiting a η of ∼750 mV (at 10 mA cm^{-2}) in alkaline media.[16,17,20,22] Despite being a moderately active electrocatalyst, birnessite can be an active water oxidation catalyst when ceric ammonium nitrate (CAN) is used as a sacrificial oxidizing agent.[14,15] The reason for this discrepancy between electrochemical water oxidation and chemical water oxidation using CAN is still under debate.[22,23]

Received: July 14, 2016
Revised: October 5, 2016
Published: October 10, 2016

DOI: 10.1021/acscatal.6b01980
ACS Catal. 2016, 6, 7739−7743

A prime motivation for the current study is to investigate whether the activity of cobalt for the OER can be further enhanced by intercalating the catalyst in the interlayer region of birnessite. A prior study from our laboratory showed that birnessite intercalated with nickel (Ni^{2+}/birnessite) was more active than either a nickel hydroxide or birnessite catalyst alone.[24] In particular, the Ni^{2+}/birnessite and nickel hydroxide catalysts exhibited a η of 420 and 550 mv (at 10 mA cm^{-1}), respectively, for the OER. Rationale for this experimental observation was based on a recent molecular dynamics (MD) simulation study.[25] This study suggested that the interaction between interlayer water molecules and intercalated metal cations in birnessite leads to a unique water structuring (i.e., frustrated water), which enhances electron transfer reactions in the interlayer. The current study aims to determine whether this strategy to increase the OER activity of a catalyst by confining it in a unique spatially confined region continues to hold true. Relative to manganese oxide, cobalt-based materials show superior activity toward OER catalysis.[8] This superior catalytic activity of cobalt-based OER catalysts is presumably due to optimal binding (i.e., not too strong and not too weak) of reaction intermediates (*OOH and *OH) on the catalytic sites that facilitate the OER.[26] Thus, cobalt was chosen as an intercalant in this study. We believe that enhancing this activity still further would be noteworthy.

Cobalt was intercalated into the interlayer of birnessite using a simple ion exchange reaction using a cobalt hydrazine complex $[Co(N_2H_4)_x(H_2O)_y]^{2+}$ (see SI for details) at room temperature. We refer to this material as Co^{2+}/birnessite. Generally, the interlayer spacing of a layered material is sensitive to the presence of guest molecules or atoms in the interlayer region.[27,28] X-ray diffraction (XRD) data presented in Figure 1 show that the (001) Bragg reflection for Co^{2+}/birnessite is shifted toward a higher two theta value relative to birnessite, indicating that the interlayer spacing of birnessite is decreased when birnessite is exposed to the cobalt hydrazine complex. The XRD data show that the interlayer spacing decreases from a value of 7.51 Å for pristine birnessite to 7.30 Å at a Co concentration of 8.4 at. % and to 7.22 Å at a Co concentration of 12.2 at. % (determined by inductively coupled plasma optical emission spectroscopy). Both scanning and transmission electron microscopy (SEM and TEM) show similar nanoflower morphologies for pristine birnessite and Co^{2+}/birnessite (Figure S1). However, a closer look at electron microscopy images reveals that there are changes in particle size before and after intercalation. We carried out Brunauer–Emmett–Teller (BET) specific surface area analysis to obtain further information. The resulting BET surface areas were 33 and 95 m^2/g for birnessite and Co^{2+}/birnessite, respectively. To confirm the spatial distribution of the intercalated Co, we performed electron energy loss spectroscopy (EELS) across a cross section of the Co^{2+}/birnessite. Figure 2a is an annular dark field (ADF) scanning transmission electron microscopy (STEM) image taken of a cross section of Co^{2+}/birnessite, where the lattice fringes of (001) plane are visible. Quantitative analysis of the relative composition of O, Mn, and Co is shown in Figure 2b. The atomic composition of each element is 59.8% ± 4.0% for O, 28.4% ± 3.3% for Mn, and 11.8% ± 3.9% for Co. The EEL spectrum collected from a line scan for quantitative analysis is displayed in Figure 2c. This particular data gives direct evidence of interlayer Co, consistent with the conclusions drawn from the XRD data. We mention that while atomic resolution STEM imaging found no evidence for structural defects in Co-free birnessite (Figure S2), it did show the presence of defects such as edge dislocations and grain boundaries after cobalt intercalation (Figure S3). As a control experiment, birnessite was exposed to hydrazine (without complexing with cobalt), and as expected it led to significant structural changes (Mn_3O_4 formation was observed, Figure S4). XRD of this material (Figure S5) showed that that the 001 reflection was at the same two-theta position as pristine birnessite. This experimental observation supports our contention that the shift of the 001 reflection associated with birnessite after exposure to cobalt/hydrazine is due to Co intercalation and a change in the interlayer spacing of birnessite. Additionally, BET specific surface area analysis on birnessite exposed to hydrazine (108 m^2/g) yielded a significant surface area enhancement. On the basis of this experimental result, we believe that the enhancement in surface area for Co^{2+}/

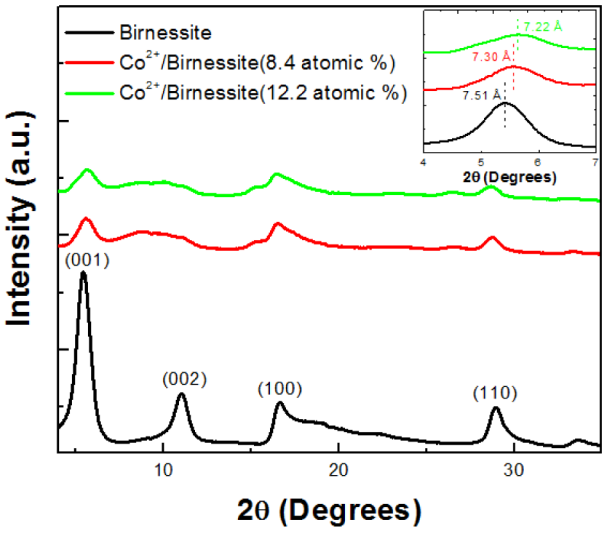

Figure 1. Powder X-ray diffraction pattern of birnessite and Co^{2+}/birnessite. The inset is the enlarged (001) reflection which indicates that interlayer spacing changes with cobalt confinement within the interlayer.

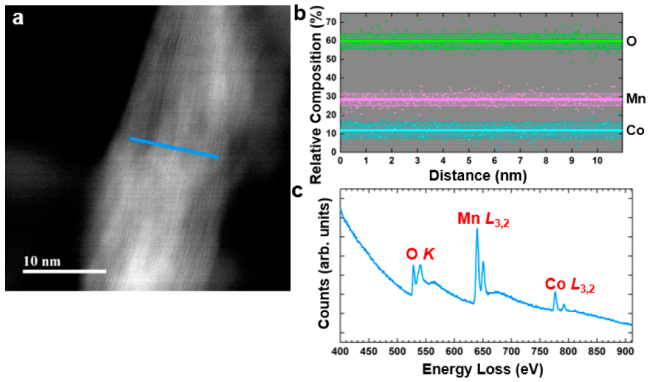

Figure 2. EELS line scan across the cross-section of the Co^{2+}/birnessite. (a) STEM ADF image of the cross section of the birnessite; (b) relative composition of O, Mn, and Co, scattered dots are original data, mean value, and standard deviation of each element are shown by solid line and dashed area; (c) EEL spectrum showing O K-edge, Mn $L_{3,2}$-edge, and Co $L_{3,2}$-edge that are used for quantitative composition analysis.

DOI: 10.1021/acscatal.6b01980
ACS Catal. 2016, 6, 7739–7743

birnessite was due to the presence of hydrazine during the intercalation process.

The oxidation state as well as chemical nature of intercalated cobalt was investigated using X-ray photoelectron spectroscopy (XPS). Figure 3a shows the Co 2p region of Co^{2+}/birnessite

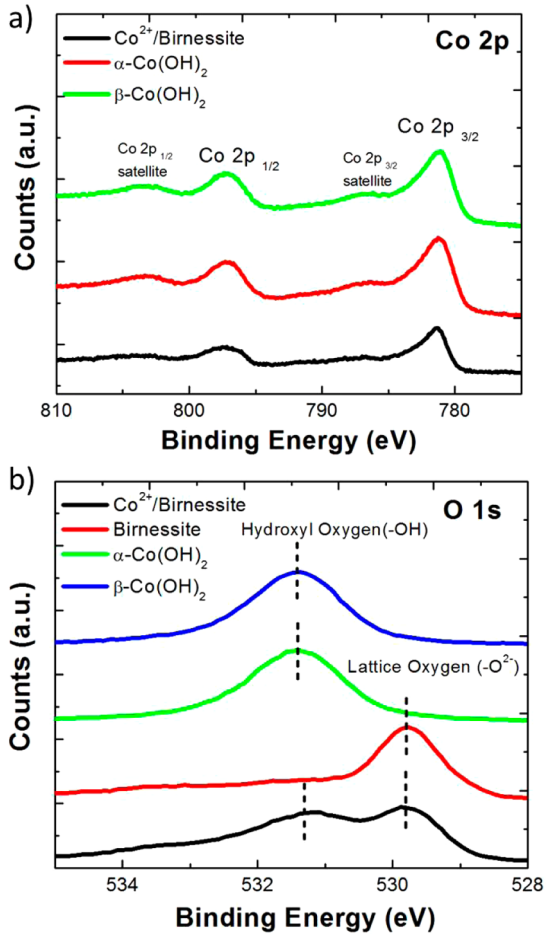

Figure 3. XPS spectra of birnessite, Co^{2+}/birnessite, α-$Co(OH)_2$ and β-$Co(OH)_2$. a) Co 2p region and b) O 1s region.

along with cobalt hydroxide standards. The similarity of the spectra suggests that the interlayer Co is in a +2 oxidation state. Based on the presence of an O 1s feature (Figure 3b) at 531.3 eV for both Co^{2+}/birnessite and $Co(OH)_2$ (absent for pristine birnessite), we propose that the intercalated Co exists at least in part as a hydroxide. Additional insight into the structure of Co^{2+}/birnessite was obtained with Raman spectroscopy. A typical Raman spectrum of birnessite exhibits two main modes at 575 cm^{-1} (in plane Mn−O vibration) and ~646 cm^{-1} (out of plane Mn−O stretching).[29] Broadening of these modes can be attributed to a disorder of the structure induced by intercalation of guest molecule or atoms in the interlayer space.[17,29] We experimentally observed such a broadening in our Raman spectra for Co^{2+}/birnessite compared to birnessite (Figure S7). We take this result as further evidence to support the notion that cobalt resides in the interlayer region of birnessite, causing structural disorder in the layered birnessite, as observed by STEM (Figures S2 and S3). Finally, XPS as well as energy-dispersive spectroscopy (Figure S8) shows that Co^{2+}/birnessite does not contain K^+, suggesting that Co^{2+} intercalation leads to the displacement of K^+ from the interlayer to maintain charge neutrality.

The electrocatalytic activity of Co^{2+}/birnessite toward OER in alkaline media (pH ~ 14) was evaluated using a typical three-electrode configuration. A catalyst ink was prepared by mixing catalyst with conductive carbon and nafion (binder). The ink was drop-cast onto a glassy carbon electrode, which was used as the working electrode (see SI for details). For comparison, the catalytic activities of α-cobalt hydroxide, β-cobalt hydroxide, cobalt oxide (Co_3O_4), cobalt substituted birnessite, and Ir/C (20 wt %) were also examined (Figure 4a).

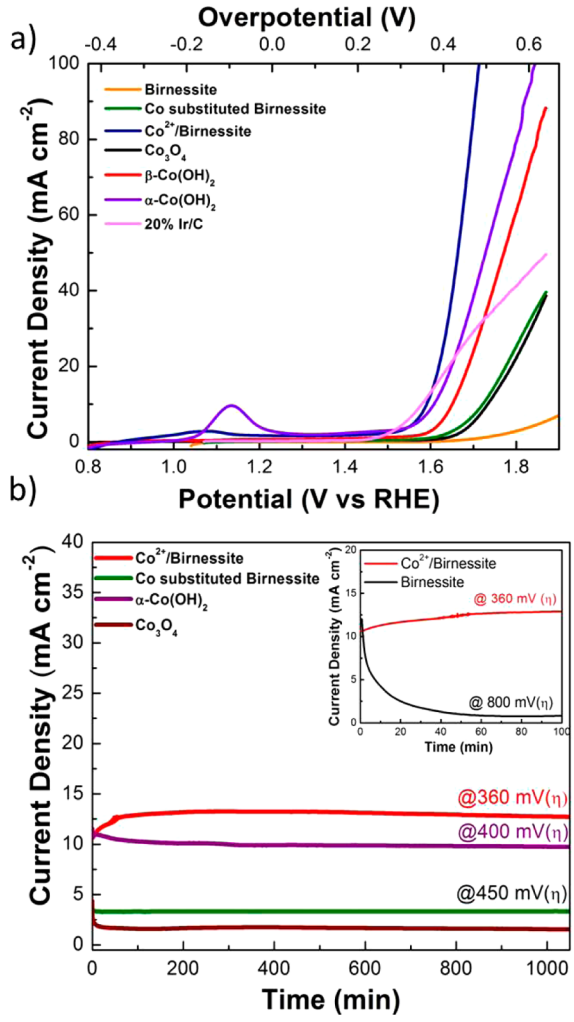

Figure 4. (a) Linear sweep voltammagrams and (b) chronoamperometry of various catalysts tested. Inset shows the chronoamperometry curve for birnessite (at η = 800 mV) in comparison with Co^{2+}/birnessite (at η = 360 mV).

The cobalt-substituted birnessite sample was prepared by synthesizing birnessite in the presence of $CoCl_2$ (see SI for details). This preparation method led to a birnessite with 12 at. % cobalt. In contrast to Co^{2+}/birnessite, XRD (Figure S9) of this material did not show a shift of the (001) reflection relative to pristine birnessite, and K^+ was not displaced during the synthesis of cobalt-substituted birnessite. These experimental observations suggested that Co^{2+} did not reside in the interlayer of this material and instead, Co^{2+} replaced manganese ions in the 2D sheets.

DOI: 10.1021/acscatal.6b01980
ACS Catal. 2016, 6, 7739−7743

Table 1. Summary of OER Activities in 1 M KOH and Atomic Ratios from ICP-OES and EDS

catalyst	confined or substituted atomic Co %	η (mV) at 10 mA cm^{-2}	TOF (s^{-1}) at η = 0.40 V	mass activity (A g^{-1}) at η = 0.40 V	Tafel slope (mV dec^{-1})
birnessite		770	0.0004	2.0	243 ± 7
Co^{2+}/birnessite	12.2	360	0.023	92	46 ± 3
Co^{2+}/birnessite	8.4	392	0.011	45	66 ± 4
Co-substituted birnessite	12.4	490	0.0023	3.0	82 ± 3
β-$Co(OH)_2$		420	0.0051	30	52 ± 3
α-$Co(OH)_2$		380	0.013	54	51 ± 4
Co_3O_4		500	0.0008	4.5	76 ± 4
20% Ir/C		350	0.018	72	72 ± 4

As shown by the polarization curves presented in Figure 4, the Co-intercalated Co^{2+}/birnessite electrocatalyst exhibits a remarkable OER activity compared to all the other catalytic materials that were tested. Co^{2+}/birnessite exhibits an η of 360 mV at a current density of 10 mA cm^{-2} with a Tafel slope of ~46 mV dec^{-1}, whereas cobalt-substituted birnessite shows an η of ~490 mV (with a Tafel slope of 82 mV dec^{-1}). This particular comparison is direct evidence to support the contention that a significant portion of OER catalysis occurs in the interlayer region.[24] Furthermore, assessment of the OER activity for 8.4 and 12.2% Co^{2+}/birnessite (Figure S10) showed that η decreased as the concentration of cobalt was increased within the interlayer region. This observation further supports the claim of interlayer cobalt being the active site for these cobalt-modified materials. Evaluation of the data compiled in Table 1 also shows that the η associated with Co^{2+}/birnessite is lower than α-$Co(OH)_2$ (380 mV), β-$Co(OH)_2$ (420 mV), and Co_3O_4 (500 mV). This additional comparison leads to the conclusion that incorporation of an active catalyst into the interlayer region of birnessite leads to an even more active catalyst, consistent with the conclusion from our prior study of Ni^{2+}/birnessite.[24]

We also conducted electrocatalytic studies at pH 7 solution conditions (using 0.5 M phosphate buffer as the electrolyte) in an effort to observe the possibility of similar enhancement due to metal intercalation (see Table S1) when H_2O was being directly oxidized (in contrast to OH^- at pH 14). Data in Figure S11 shows that at pH 7, as expected, the OER activity for the different electrocatalysts are suppressed relative to their performance in an alkaline medium, consistent with prior studies[30,31] with transition-metal-oxide OER catalysts. More important to the focus of this contribution is that the trend in OER activity for different electrocatalysts is similar to the trend obtained in an alkaline medium (η for OER for Co^{2+}/birnessite < cobalt hydroxides < birnessite). These results taken together with the pH 14 results suggest that the superior activity of Co^{2+}/birnessite (relative to pure $Co(OH)_2$ phases) is maintained whether H_2O or OH^- is the dominant species being oxidized.

To further support the validity of our conclusions, we determined the electrochemically active surface area (ECSA) of the electrocatalysts. Because the double layer capacitance (C_{dl}) of an electrocatalyst is proportional to ECSA, one can investigate C_{dl} to estimate the ECSA. Figure S12 depicts C_{dl} values for the different catalysts tested. The absence of a significant enhancement in C_{dl} for Co^{2+}/birnessite suggests that the improved OER activity is not primarily due to surface-area-related phenomena (Figure S12) but instead is due to favorable interactions of interlayer water with intercalated cobalt toward OER. Moreover, electrochemical investigation of birnessite exposed to hydrazine (Figure S13) revealed that there is no enhancement in OER activity even with the significant enhancement in surface area. Thus, we believe that the increased activity of Co^{2+}/birnessite for the OER is not attributable to an increased surface area but rather due to cobalt active sites in the interlayer. Furthermore, inspection of polarization curves for Co^{2+}/birnessite and cobalt hydroxides reveal that the oxidation of Co^{2+} to Co^{3+} occurs at a lower potential (1.07 V vs RHE) for Co^{2+}/birnessite relative to cobalt hydroxide (1.13 V vs RHE). Consistent with this experimental observation are previously mentioned MD simulations[24,25] for Ni^{2+}/birnessite that suggested that there is a lowering of the barrier for electron transfer for a metal cation (e.g., Ni^{2+}) coordinated by interlayer water compared to the same metal cation coordinated by bulk water. In analogy with the current results for the Co^{2+}/Co^{3+} couple, it was shown in the earlier work that Ni^{2+} oxidized to Ni^{3+} at a lower potential when it was intercalated in birnessite than when it was present in bulk $Ni(OH)_2$. This phenomenon[24] was proposed to be due to frustrated water in the interlayer of birnessite. In essence, if interlayer cations are abundant, coordination of water to the cation to form a complete solvation shell is hindered resulting in enhanced solvent fluctuations (i.e., frustrated) as individual water molecules seek to align their dipoles with interlayer cations. These enhanced fluctuations of interlayer water lower the reorganization energy for electron transfer reactions.[19,20]

As illustrated by Table 1, the improved OER activity of Co^{2+}/birnessite is further emphasized by turnover frequencies (TOF) and mass activities. Specifically, Co^{2+}/birnessite (TOF ~ 0.02 s^{-1}) shows an order of magnitude improvement in TOF relative to cobalt-substituted birnessite (TOF ~ 0.002 s^{-1}). Furthermore, the Faradaic efficiency (~99%) was determined by performing electrolysis at a constant current using an airtight H-type cell, and evolved oxygen was analyzed using gas chromatography (SI Figure S14). In order to evaluate the stability of the catalyst, chronopotentiometry (at constant current of 20 mA cm^{-2}) and chronoamperometry (at 360 mV overpotential) were performed, and the Co^{2+}/birnessite catalyst was stable for more than 24 h (Figure 4b and S15). Additionally, electrochemical redox cycling was performed on this cobalt-confined birnessite, and even after 1000 cycles, no degradation of catalytic activity was experimentally observed (Figure S16).

In closing, we mention that the results presented in this contribution for Co^{2+}/birnessite taken together with those published elsewhere for Ni^{2+}/birnessite further emphasize the unique interlayer environment of birnessite. In short, both Co^{2+} and Ni^{2+}, when intercalated in birnessite, exhibit a lowering of their respective oxidation potentials and an enhancement in their activity toward the OER. In stark contrast, the simple

DOI: 10.1021/acscatal.6b01980
ACS Catal. 2016, 6, 7739−7743

substitution of Co^{2+} into the octahedrally coordinated sheets of birnessite or adsorption of Ni^{2+} on the octahedral sheets of birnessite[24] does not lead to the enhancements in OER activity that are observed when the metal cations are intercalated. Ongoing research in our laboratory is further investigating the unique chemical environment of the interlayer with experiment, MD simulations, and theory.

■ ASSOCIATED CONTENT

Supporting Information

The Supporting Information is available free of charge on the ACS Publications website at DOI: 10.1021/acscatal.6b01980.

Experimental details, XPS, Raman spectra, LSV polarization curves, and electron microscopy (PDF)

■ AUTHOR INFORMATION

Corresponding Author

*E-mail: dstrongi@temple.edu.

Notes

The authors declare no competing financial interest.

■ ACKNOWLEDGMENTS

This work was supported as part of the Center for the Computational Design of Functional Layered Materials, an Energy Frontier Research Center funded by the U.S. Department of Energy, Office of Science, Basic Energy Sciences under Award No. DE-SC0012575 (paper concept, synthesis, XRD, electrochemistry, and Raman). Y.Z. was supported by DOE-BES, MSE, under Contract No. DE-SC0012704 (cross sectional EELS and high resolution inverted ADF imaging). The XPS measurements carried out at the University of Delaware surface analysis facility were supported by NSF (Grant 1428149) and the NIH NIGMS COBRE program (Grant P30-GM110758).

■ REFERENCES

(1) Gray, H. B. *Nat. Chem.* **2009**, *1*, 7−7.
(2) Lewis, N. S.; Nocera, D. G. *Proc. Natl. Acad. Sci. U. S. A.* **2006**, *103*, 15729−15735.
(3) Nocera, D. G. *Acc. Chem. Res.* **2012**, *45*, 767−776.
(4) Caban-Acevedo, M.; Stone, M. L.; Schmidt, J. R.; Thomas, J. G.; Ding, Q.; Chang, H.-C.; Tsai, M.-L.; He, J.-H.; Jin, S. *Nat. Mater.* **2015**, *14*, 1245−1251.
(5) Callejas, J. F.; Read, C. G.; Popczun, E. J.; McEnaney, J. M.; Schaak, R. E. *Chem. Mater.* **2015**, *27*, 3769−3774.
(6) Cheng, L.; Huang, W.; Gong, Q.; Liu, C.; Liu, Z.; Li, Y.; Dai, H. *Angew. Chem., Int. Ed.* **2014**, *53*, 7860−7863.
(7) Shi, J.; Hu, J.; Luo, Y.; Sun, X.; Asiri, A. M. *Catal. Sci. Technol.* **2015**, *5*, 4954−4958.
(8) Jung, S.; McCrory, C. C. L.; Ferrer, I. M.; Peters, J. C.; Jaramillo, T. F. *J. Mater. Chem. A* **2016**, *4*, 3068−3076.
(9) Lee, Y.; Suntivich, J.; May, K. J.; Perry, E. E.; Shao-Horn, Y. *J. Phys. Chem. Lett.* **2012**, *3*, 399−404.
(10) Zhang, B.; Zheng, X.; Voznyy, O.; Comin, R.; Bajdich, M.; García-Melchor, M.; Han, L.; Xu, J.; Liu, M.; Zheng, L.; García de Arquer, F. P.; Dinh, C. T.; Fan, F.; Yuan, M.; Yassitepe, E.; Chen, N.; Regier, T.; Liu, P.; Li, Y.; De Luna, P.; Janmohamed, A.; Xin, H. L.; Yang, H.; Vojvodic, A.; Sargent, E. H. *Science* **2016**, *352*, 333−337.
(11) Li, W.; He, D.; Sheehan, S. W.; He, Y.; Thorne, J. E.; Yao, X.; Brudvig, G. W.; Wang, D. *Energy Environ. Sci.* **2016**, *9*, 1794−1802.
(12) Sala, X.; Romero, I.; Rodríguez, M.; Escriche, L.; Llobet, A. *Angew. Chem., Int. Ed.* **2009**, *48*, 2842−2852.
(13) Duan, L.; Bozoglian, F.; Mandal, S.; Stewart, B.; Privalov, T.; Llobet, A.; Sun, L. *Nat. Chem.* **2012**, *4*, 418−423.
(14) Boppana, V. B. R.; Yusuf, S.; Hutchings, G. S.; Jiao, F. *Adv. Funct. Mater.* **2013**, *23*, 878−884.
(15) McKendry, I. G.; Kondaveeti, S. K.; Shumlas, S. L.; Strongin, D. R.; Zdilla, M. J. *Dalton Trans.* **2015**, *44*, 12981−12984.
(16) Meng, Y.; Song, W.; Huang, H.; Ren, Z.; Chen, S. Y.; Suib, S. L. *J. Am. Chem. Soc.* **2014**, *136*, 11452−11464.
(17) Thenuwara, A. C.; Shumlas, S. L.; Attanayake, N. H.; Cerkez, E. B.; McKendry, I. G.; Frazer, L.; Borguet, E.; Kang, Q.; Zdilla, M. J.; Sun, J.; Strongin, D. R. *Langmuir* **2015**, *31*, 12807−12813.
(18) Baricuatro, J. H.; Saadi, F. H.; Carim, A. I.; Velazquez, J. M.; Kim, Y.-G.; Soriaga, M. P. *J. Phys. Chem. C* **2016**, *120*, 15618−15631.
(19) Lee, S. Y.; González-Flores, D.; Ohms, J.; Trost, T.; Dau, H.; Zaharieva, I.; Kurz, P. *ChemSusChem* **2014**, *7*, 3442−3451.
(20) Nakayama, M.; Fujii, Y.; Fujimoto, K.; Yoshimoto, M.; Kaide, A.; Saeki, T.; Asada, H. *RSC Adv.* **2016**, *6*, 23377−23382.
(21) Huynh, M.; Shi, C.; Billinge, S. J. L.; Nocera, D. G. *J. Am. Chem. Soc.* **2015**, *137*, 14887−14904.
(22) Pokhrel, R.; Goetz, M. K.; Shaner, S. E.; Wu, X.; Stahl, S. S. *J. Am. Chem. Soc.* **2015**, *137*, 8384−8387.
(23) Wiechen, M.; Najafpour, M. M.; Allakhverdiev, S. I.; Spiccia, L. *Energy Environ. Sci.* **2014**, *7*, 2203−2212.
(24) Thenuwara, A. C.; Cerkez, E. B.; Shumlas, S. L.; Attanayake, N. H.; McKendry, I. G.; Frazer, L.; Borguet, E.; Kang, Q.; Remsing, R. C.; Klein, M. L.; Zdilla, M. J.; Strongin, D. R. *Angew. Chem., Int. Ed.* **2016**, *55*, 10381−10385.
(25) Remsing, R. C.; McKendry, I. G.; Strongin, D. R.; Klein, M. L.; Zdilla, M. J. *J. Phys. Chem. Lett.* **2015**, *6*, 4804−4808.
(26) Man, I. C.; Su, H. Y.; Calle-Vallejo, F.; Hansen, H. A.; Martínez, J. I.; Inoglu, N. G.; Kitchin, J.; Jaramillo, T. F.; Nørskov, J. K.; Rossmeisl, J. *ChemCatChem* **2011**, *3*, 1159−1165.
(27) Lu, Z.; Wang, H.; Kong, D.; Yan, K.; Hsu, P.-C.; Zheng, G.; Yao, H.; Liang, Z.; Sun, X.; Cui, Y. *Nat. Commun.* **2014**, *5*, ArticleNo. 4345.
(28) Motter, J. P.; Koski, K. J.; Cui, Y. *Chem. Mater.* **2014**, *26*, 2313−2317.
(29) Julien, C.; Massot, M.; Baddour-Hadjean, R.; Franger, S.; Bach, S.; Pereira-Ramos, J. P. *Solid State Ionics* **2003**, *159*, 345−356.
(30) Gardner, G.; Al-Sharab, J.; Danilovic, N.; Go, Y. B.; Ayers, K.; Greenblatt, M.; Charles Dismukes, G. *Energy Environ. Sci.* **2016**, *9*, 184−192.
(31) Kim, H.; Park, J.; Park, I.; Jin, K.; Jerng, S. E.; Kim, S. H.; Nam, K. T.; Kang, K. *Nat. Commun.* **2015**, *6*, Article No. 8253.

DOI: 10.1021/acscatal.6b01980
ACS Catal. 2016, 6, 7739−7743